

# Performance analysis of FSO link resilience through integrated MIMO and homodyne detection techniques for various cloud circumstances

YOGESH KUMAR GUPTA\*, ADITYA GOEL

*Department of Electronics and Communication Engineering, Maulana Azad National Institute of Technology, Bhopal, Madhya Pradesh, India*

Free space optics (FSO) system facilitates the transmission of message signals through the atmosphere, providing numerous advantages. In spite of this, the efficiency of FSO across long distances is restricted by the presence of a variety of cloud situations. This research examines the effectiveness of FSO module under various cloud conditions. It proposes a wavelength division multiplexing (WDM) methodology, combined with multiple-input multiple-output (MIMO) techniques. Furthermore, it utilizes homodyne detection in the receiver section. The suggested framework achieves transmission ranges under various cloud conditions: 108 m under cumulus clouds, 223 m under stratus clouds conditions, 330 m under stratocumulus clouds conditions, 140 m under altostratus clouds conditions, 160 m under nimbostratus clouds conditions, 130 km under cirrus clouds conditions, and 200 km under thin cirrus conditions. Performance assessment is a comprehensive examination of critical parameters such as Bit Error Rate (BER) and Q factor to fully evaluate system performance.

(Received July 30, 2024; accepted February 3, 2025)

*Keywords:* Homodyne detection, Q factor, FSO, Clouds circumstances, BER

## 1. Introduction

Global internet connectivity continues to grow in underserved locations by using optical wireless technologies to fulfil the changing needs of wireless networks. Presently, physical links are the prevailing modes of broadband connectivity [1]. Cable structure ensures a reliable connection irrespective of the weather but involves considerable costs, particularly in the last link because of the use of a point-to-point design. On the other hand, RF connections provide weather independent working and do not depend on point-to-point scenarios [2-3]. Nevertheless, in its present state there are difficulties, and these are due to the high degree of utilization and the expensive fees for using RF technologies. The transfer of data from two points using light beams is called FSO technology. This technology employs optical sources and detectors to communicate signals between transceiver nodes through the aerial free-space path. In next generation network, FSO has some benefits over the radio frequency links. These benefits includes operation in a secure and license free band, high bandwidth capacity, efficient space reuse, no electromagnetic compatibility, interference problem and low power consumption per bit. But it is necessary to underline here that, in order to work properly, an optical wireless link requires an unobstructed LOS connection and highly accurate alignment inside communicating nodes [4-5].

FSO system faces several challenges like atmospheric turbulence, and weather conditions such as rain, fog, snow, dust & haze. Many research works have carried out

comprehensive analyses to determine the efficiency of FSO systems in various environmental. Ref. [6] analyzed the performance of FSO module with rain, fog and dust climatic conditions and achieved transmission range of 0.125 km in severe dust environments. M. Mrabet et al. [7] employed the effectiveness of the FSO module in the desert area and foggy climate conditions. In this study [7], the obtain transmission range was 2.4, 1.75, and 0.8 km for light, medium, and high foggy conditions, respectively. S. Sinha et al. [8] examined the FSO module performance in rainy and wet-snowy condition and achieved transmission distance of 2.5 km.

The effectiveness assessment of FSO systems was conducted using several methodologies. These approaches encompassed by various techniques designed for assessing FSO system reliability in specific aspects. Anuranjana et al. [9] used a mode division multiplexing along with WDM as a technique to enhance the capacity and performance of the FSO system. In Ref. [10], polarization division multiplexing and spectrum slicing WDM techniques were used together to examine the performance of FSO system under different weather conditions including rainy, foggy, snowy and so on. Ref. [11] employes dense WDM technique for the assessment of FSO system. The study used various modulation techniques, attaining the throughput of 2.5 Gbps on individual channels. To evaluate the performance of the FSO module based on orbital angular moment, Mehtab et al. [12] proposed various modulation techniques. The results suggested NRZ modulation techniques performed better compared to other modulation schemes. Farouk et

al. [13] conducted an assessment of the FSO module's performance based on the use of  $2 \times 2$  FSO transceiver modules. N. Rani et al. [14], used a  $4 \times 4$  FSO transceiver modules to improve the efficiency of the FSO module. The OFDM, spectral amplitude coding, mode division multiplexing, optical code division multiple access and dense WDM techniques were employed with FSO module in Ref. [15-17]. G. G. Soni et al. [18] performed experimental analyses of environmental conditions like rainfall, on FSO links. In our previous work [19-21], we investigated the performance of the FSO module under all weather conditions. We have used multiple beams and WDM techniques across all these conditions. Thus, using these methods, we aimed to eliminate the problems caused by the atmospheric and the environment turbulence, which can negatively affect signal quality and transmission rate. The studies conducted by us shows the effectiveness of this hybrid approach which are presented in current and previous findings to enhancements of transmission range.

## 2. Research shortcomings and primary contributions

The literature review conducted in the present work identifies different methods employed to address different types of climates within the FSO module. Currently, there is a lack of thorough studies that encounter the challenges caused by changing clouds conditions in the FSO system. This research gap limits the performance and reliability of FSO system in various clouds conditions. It's important to explore this area to understand how clouds conditions, affects overall performance of the FSO system. Investigating these factors can prove helpful for better understanding of FSO systems so as to lessen the impact of the clouds interference and increase the stability and resilience of the system in different environments. The primary goal of the current study is a comprehensive

assessment of the FSO system's performance in different clouds conditions.

This work uses the integration of WDM with homodyne detection and MIMO techniques. The evaluation of this integration is conducted using the optisystem tool, highlighting the principal contributions of this endeavour, as delineated below:

i) We have developed a highly efficient WDM-based framework, employing homodyne detection to mitigate the effects of various cloud conditions. By utilizing single-parameter optimization (SPO), we have fine-tuned the system's attributes, while integrating the MIMO technique has improved the performance of the channel component.

ii) Calculations have been performed to assess the attenuation levels under various cloud conditions, including cumulus, stratus, stratocumulus, altostratus, nimbostratus, cirrus, and thin cirrus. This involved analyzing how differing cloud densities, compositions, and altitudes impact signal attenuation within the optical communication system.

iii) We conduct simulations to ascertain how varying types and densities of clouds influence the transmission range, ensuring our framework reliably transmits data.

iv) The findings indicate that the transmission range is superior under thin cirrus cloud conditions compared to other cloud conditions.

This study comprises five main sections. The Introductory part evaluates the significance of FSO connections through a literature review. Section 2, "Methodology," discusses the suggested system layout. Section 3 covers the variables and their respective settings utilized in the simulation. In Section 4, the results of implementing the framework are elaborated upon. Lastly, the research is finally concluded in the Conclusion Section, which also addresses future work on the suggested framework.

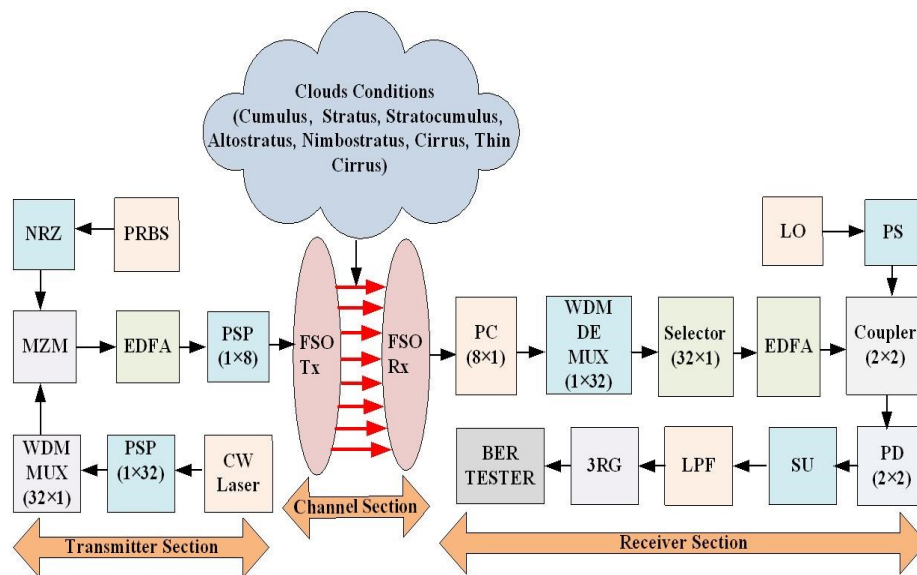


Fig. 1. Proposed MIMO FSO framework for incorporating different cloud circumstance (colour online)

### 3. Methodology analysis

The block schematic depicted in Fig. 1 illustrates the suggested FSO framework, which is based on homodyne detection. This section examines the broad discussion of the system's intricacies, specifically examining the multi-stage process it entails. In this system "Pseudo Random Bit Sequence generator" is denoted as "PRBS", the "Mach-Zehnder modulator" is denoted by "MZM", the continuous wave laser is referred as "CW Laser", "PSP" stands for power splitter, "WDM MUX" stands for wavelength division multiplexer, "LO" corresponds to the local oscillator, "PS" represents the phase shifter, "PC" denotes the power combiner, "WDM DEMUX" signifies the wavelength division demultiplexer, "PD" denoted as PIN photodetector, "SU" refers to the subtractor, "LPF" refers the low pass filter, and "3RG" abbreviates 3R regenerator. These abbreviations collectively contribute to describing the various components and functionalities embedded in the proposed FSO framework.

#### 3.1. Transmitting module

The transmitter module depicted in Fig. 1 utilizes a PRBS to generate random bits for transmission. The conversion of these bits into a digital signal is accomplished through the use of an NRZ pulse generator. Conversely, CW laser emits uninterrupted light with diverse intensities; specifically, it produces high-intensity light for the binary digit 1 and low-intensity light for the binary digit 0. The PS ( $1 \times 32$ ) divides the optical signal into 32 signals as outputs. Following this, the signal undergoes multiplexing through the utilization of a WDM Multiplexer with a configuration of 32 inputs to 1 output. This process involves combining multiple signals of different wavelengths onto a single optical fibre, allowing for efficient transmission and utilization of the available bandwidth, after which the signal is multiplex with a WDM MUX ( $32 \times 1$ ). The acquired signal is strengthened by the EDFA. The complete signal is then separated into eight distinct output signals by the PSP ( $1 \times 8$ ). Later, this signal is transmitted over the communication medium via the FSO Tx module.

#### 3.2. Channel module

In this module, the FSO Tx component sends out eight beams. The channel is subject to turbulence losses induced by diverse cloud conditions such as cumulus, stratus, stratocumulus, altostratus, nimbostratus, cirrus, and thin cirrus, each contributing to varying levels of signal disruption.

For the purpose of determining the Aerosol/Mie scattering attenuation coefficient  $\xi_a(\lambda)$  at a specific wavelength, Kruse [22] devised a mathematical formula, Eq. (1).

$$\xi_a(\lambda) = \frac{3.912}{\delta} \left( \frac{\lambda}{550(nm)} \right)^{-p} \quad (1)$$

In the context of Eq. (1),  $p$  signifies the diversity of particle dimensions involved in scattering, and  $\delta$  denotes the visibility. The value of  $p$  is subject to change based on the visibility, as described by Eq. (2).

$$p = \begin{cases} 1.6 & \delta > 50 \text{ km} \\ 1.3 & 6 \text{ km} < \delta < 50 \text{ km} \\ 0.585 \delta^{1/3} & \delta < 6 \text{ km} \end{cases} \quad (2)$$

In the model proposed by Kruse [22], the particles are assumed to be significantly smaller in size compared to the wavelength. However, to meet specific requirements, Kim [23] made modifications to this model, as indicated by Eq. (3).

$$p = \begin{cases} 1.6 & \delta > 50 \text{ km} \\ 1.3 & 6 \text{ km} < \delta < 50 \text{ km} \\ 0.16 \delta + 0.34 & 1 \text{ km} < \delta < 6 \text{ km} \\ \delta - 0.5 & 0.5 \text{ km} < \delta < 1 \text{ km} \\ 0 & \delta < 0.5 \text{ km} \end{cases} \quad (3)$$

This study calculates attenuation using the Kim model [23] under various cloud conditions. These models incorporate Eq. (4) [4-5] to compute the visibility, considering the cloud's liquid water content ( $Q$ ) and number density ( $R$ ). The visibility value is substituted into Eq. (1) and the  $\xi_a(\lambda)$  is calculated. The compositions employed for each cloud type are displayed in Table 1. Table 1 shows the parameter  $\xi_a(\lambda)$  is highly sensitive to cloud type, with cumulus clouds exhibiting the highest attenuation  $\xi_a(\lambda)=604.6507$ . On the other hand, cirrus and thin cirrus clouds, characterized by low water content and small droplet concentration, show minimal attenuation  $\xi_a(\lambda)=0.0501$  and  $\xi_a(\lambda)=0.0111$ , respectively.

$$\delta = \frac{1.002}{(Q+R)^{0.6473}} \quad (4)$$

Table 1 Compositions of various cloud types [4-5]

Type of Clouds	$Q$ (g/m <sup>3</sup> )	$R$ (cm <sup>-3</sup> )	$\xi_a(\lambda)$
Cumulus	1	250	604.6507
Stratus	0.29	250	271.3406
Stratocumulus	0.15	250	177.08771
Altostratus	0.41	400	460.24217
Nimbostratus	0.65	200	395.98025
Cirrus	0.06405	0.025	0.050097261
Thin cirrus	0.000313	0.5	0.011114682

To improve the efficacy of the FSO system, this study employs the MIMO ( $8 \times 8$  beams) technique in the channel module. Finally, the FSO receiver (FSO Rx) module acquires this optical signal. Furthermore, the utilization of the Gamma-Gamma model has been implemented in the channel section. The PDF for this model is represented by Eq. (5) [24].

$$g_{L_a}(L_a) = \frac{2(cd)^{\frac{c+d}{2}}}{\Gamma(c)\Gamma(d)} L_a^{\frac{(c+d)}{2}-1} K_{c-d}(2\sqrt{cdL_a}) \quad (5)$$

The modified Bessel function of the second kind is denoted as  $K_{c-d}(\dots)$ . In this context, ' $c$ ' and ' $d$ ' represent the quantity of small and large-scale eddies, respectively, in this scenario. Equations. (6a) and (6b) establish  $c$  and  $d$ , respectively.

$$c = \left[ \text{Exp} \left( \frac{0.49\sigma_r^2}{(1+1.11\sigma_r^{12/5})^{7/6}} \right) - 1 \right]^{-1} \quad (6a)$$

$$d = \left[ \text{Exp} \left( \frac{0.51\sigma_r^2}{(1+0.69\sigma_r^{12/5})^{5/6}} \right) - 1 \right]^{-1} \quad (6b)$$

The symbol  $\sigma_r^2$  Denotes the Rytov variance, which acts as a measure of turbulence intensity within the channel. The determination of the value of  $\sigma_r^2$  Is facilitated by employing Eq. (7).

$$\sigma_r^2 = 1.23C_n^2 k^{7/6} r^{11/6} \quad (7)$$

The refractive index structure parameter symbolized as  $C_n^2$ , signifies the intensity of atmospheric turbulence. Its magnitudes vary with both the wave number ( $k$ ) and the distance of the link ( $r$ ).

Table 2. Various parameters and their associated values

Parameters	Values
Frequency	193.1 thz
Power	20 dbm
Channel	32
Bit rate (per channel)	10 Gbps
Attenuation of cumulus cloud condition	604.651 dB/km
Attenuation of stratus cloud condition	271.341 dB/km
Attenuation of stratocumulus cloud condition	177.088 dB/km
Attenuation of altostratus cloud condition	460.242 dB/km
Attenuation of nimbostratus cloud condition	395.98 dB/km
Attenuation of cirrus cloud condition	0.0501 dB/km
Attenuation of thin cirrus cloud condition	0.01111 dB/km
Aperture diameter of Transmitter	5 cm [25]
Aperture diameter of Receiver	20 cm [25-26]
Transmission Range	0.1-200 km
Responsivity	1 A/W
Dark Current	10 na

### 3.3. Receiving module

The utilization of a demultiplexer is integral to the reversal of the operation illustrated in Fig. 1. At the receiver end, a coherent laser source is employed to generate the carrier signal essential for this procedure. This signal undergoes a series of transformations facilitated by a PS and EDFA to achieve a  $\pi/2$  Phase shift and amplification, respectively. Subsequently, the modulated signal is conveyed to a photodetector through an optical coupler ( $2 \times 2$ ). Furthermore, the output signal is detected by PIN PD featuring a responsivity of 1 A/W, alongside a dark current of 10 na. The outputs of the PD and the coupler are combined within a subtractor block, following which the resultant signal is refined through the implementation of an LPF. Finally, the system's efficacy is evaluated through the BER tester.

### 4. Proposed framework simulation design

Table 2 provides a detailed overview of the system parameters, including their respective values and units. The optimization process for the proposed framework is accomplish using a SPO method. This method allows for fine-tuning various parameters to enhance the overall performance and efficiency of the system.

### 5. Results and discussion

In this part, we provide a thorough comparative investigation, examining the efficacy of the proposed framework across various cloud conditions. This assessment aims to elucidate how the performance of the framework varies under diverse atmospheric scenarios characterized by different cloud types.

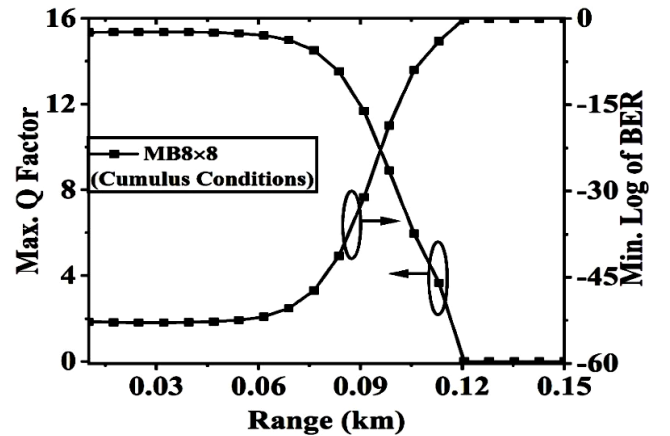


Fig. 2. Assessing the  $Q$  factor and BER for the suggested framework under cumulus cloud conditions

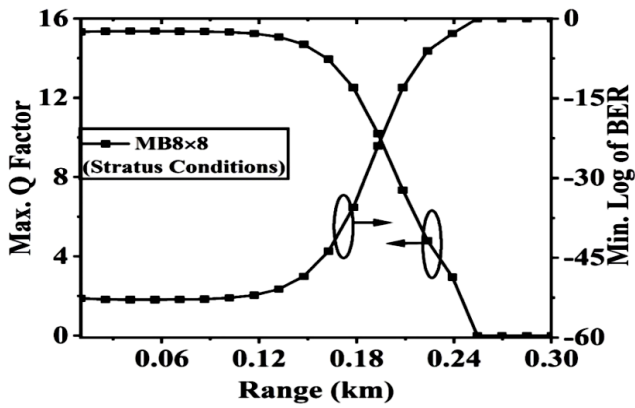


Fig. 3. Assessing the Q factor and BER for the suggested framework under stratus cloud conditions

**5.1. Outcomes in the presence of cumulus clouds conditions (Attenuation = 604.651 dB/km):**

Fig. 2 presents the outcomes under the conditions of cumulus clouds (with an attenuation of 604.651 db/km). According to the findings, a maximum reachable range of 108 m is possible while maintaining acceptable BER and Q Factor values.

**5.2. Outcomes in the presence of stratus clouds conditions (Attenuation = 271.341 dB/km):**

Fig. 3 displays the outcomes under the conditions of stratus clouds, with an attenuation of 271.341 dB/km. The findings indicate a maximum reachable range of 223 meters, alongside acceptable BER and Q Factor values.

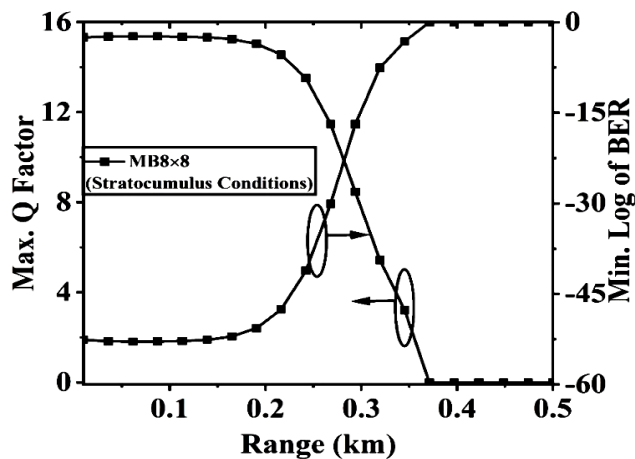


Fig. 4. Assessing the Q factor and BER for the suggested framework under stratocumulus cloud conditions

**5.3. Outcomes in the presence of stratocumulus clouds conditions (Attenuation = 177.088 dB/km):**

The outcomes under the conditions of stratocumulus clouds, with an attenuation of 177.088 dB/km, are depicted in Fig. 4. These results reveal a maximum reachable range of 330 meters while maintaining acceptable BER and Q Factor values.

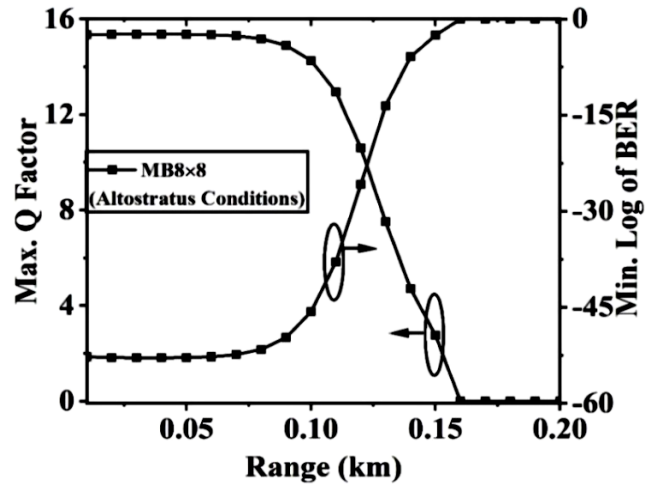


Fig. 5. Assessing the Q factor and BER for the suggested framework under altostratus clouds conditions

**5.4. Outcomes in the presence of altostratus clouds conditions (Attenuation = 460.242 dB/km):**

Fig. 5 showcases the outcomes under the conditions of altostratus clouds, with an attenuation of 460.242 dB/km. The findings indicate a maximum reachable range of 140 meters, accompanied by acceptable BER and Q Factor values.

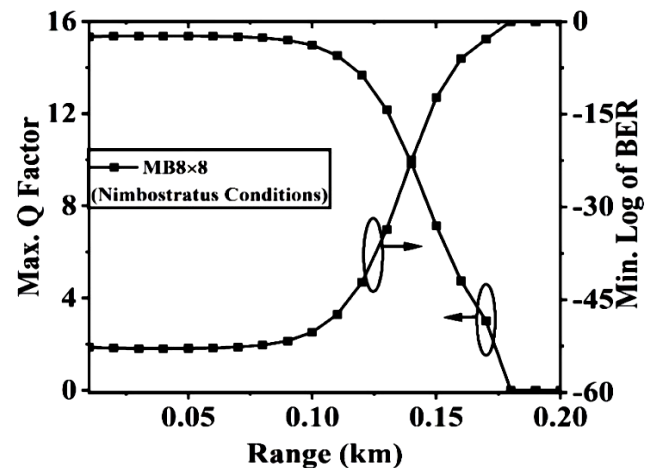


Fig. 6. Assessing the Q factor and BER for the suggested framework under nimbostratus clouds conditions

### 5.5. Outcomes in the presence of nimbostratus clouds conditions (Attenuation = 395.98 dB/km):

The outcomes under the conditions of nimbostratus clouds, with an attenuation of 395.98 dB/km, are presented in Fig. 6. These results demonstrate a maximum reachable range of 160 meters while maintaining acceptable BER and Q Factor values.

### 5.6. Outcomes in the presence of cirrus clouds conditions (Attenuation = 0.0501 dB/km):

Fig. 7 illustrates the outcomes under the conditions of cirrus clouds, with an attenuation of 0.0501 dB/km. According to these findings, a maximum reachable range of 130 kilometres is achievable while maintaining acceptable BER and Q Factor values.

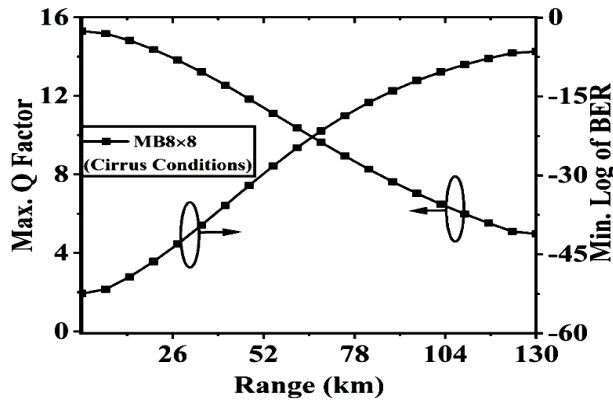


Fig. 7. Assessing the Q factor and BER for the suggested framework under cirrus clouds conditions

### 5.7. Outcomes in the presence of thin cirrus clouds conditions (Attenuation = 0.01111 dB/km):

The outcomes under the conditions of thin cirrus clouds, with an attenuation of 0.01111 dB/km, are presented in Fig. 8. These results indicate a maximum reachable range of 200 kilometres while maintaining acceptable BER and Q Factor values.

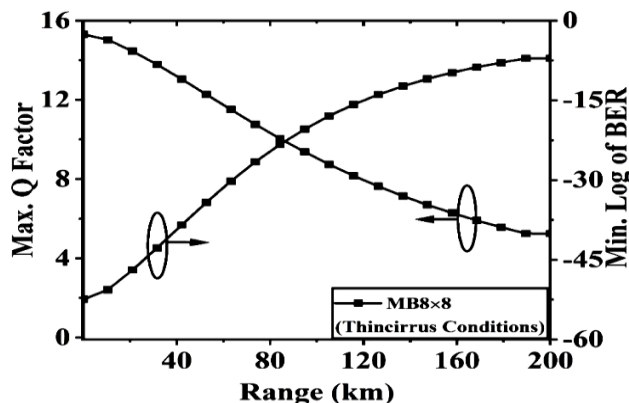


Fig. 8. Assessing the Q factor and BER for the suggested framework under thin cirrus cloud conditions

## 6. Conclusion

This research provides a comprehensive approach to reducing the effects of various cloud conditions to the FSO system. The suggested framework attains a channel capacity of 320 Gbps. Additionally, this study indicates its performance is superior under thin cirrus cloud conditions when compared to other cloud types such as cumulus, stratus, stratocumulus, altostratus, nimbostratus, and cirrus clouds. This architecture demonstrates significant potential for enhancing optical-wireless networks, thereby increasing communication range and channel capacity. The findings of this study can serve as a valuable resource in establishing secure and high-speed communication links between military installations. This enables a reliable means of transmitting sensitive data over long distances without relying on physical cables or vulnerable radio frequencies. Ultimately, this advancement strengthens the military's capability to coordinate operations, share intelligence, and maintain situational awareness across various environments.

## References

- [1] A. K. Majumdar, *Advanced free space optics (FSO): A Systems Approach*, Springer Series in Optical Sciences Book **186** (2014).
- [2] G. Pandey, A. Goel, *Opt. Quant. Electron.* **47**, 3445 (2015).
- [3] G. Pandey, A. Goel, *Optik* **125**(17), 4951 (2014).
- [4] M. S. Awan, E. Leitgeb, B. Hillbrand, F. Nadeem, M. S. Khan, 2009 International Workshop on Satellite and Space Communications, IEEE, 274 (2009).
- [5] E. Erdogan, I. Altunbas, G. K. Kurt, M. Bellemare, G. Lamontagne, H. Yanikomeroğlu, *IEEE Access* **9**, 31179 (2021).
- [6] S. V. M. Y. Naga, A. Sivanantha Raja, K. Esakki, Muthu, *Optoelectron. Adv. Mat.* **17**(9-10), 446 (2023).
- [7] M. Mrabet, M. Sliti, *Opt. Quant. Electron.* **56**(4), 659 (2024).
- [8] S. Sinha, C. Kumar, *Wireless Personal Commun.* **133**(4), 2411 (2023).
- [9] S. Kaur, R. Goyal, S. Chaudhary, *Optik* **257**, 168809 (2022).
- [10] E. Vasani, V. Shah, *Wireless Personal Commun.* **130**(2), 777 (2023).
- [11] E. E. Elsayed, D. Kakati, M. Singh, A. Grover, G. Anand, *Opt. Quant. Electron.* **54**(11), 768 (2022).
- [12] M. Singh, A. Atieh, A. Grover, O. Barukab, *Alexandria Engineering Journal* **61**(7), 5203 (2022).
- [13] F. K. Shaker, M. A. A. Ali, *Journal of Optical Communications* **42**(2), 235 (2021).
- [14] N. Rani, P. Singh, P. Kaur, *Optik* **24**, 168165 (2021).
- [15] M. Singh, J. Kříž, M. M. Kamruzzaman, V. Dhasarathan, A. Sharma, S. A. Abd El-Mottaleb, *Front. Phys.* **10**(5), 934848 (2022).
- [16] M. Singh, S. Chebaane, S. B. Khalifa, A. Grover, S. Dewra, M. Angurula, *Front. Phys.* **9**(3), 746779

- (2021).
- [17] K. Singh, M. Singh, A. Grover, Optoelectron. Adv. Mat. **18**, 134 (2024).
- [18] G. G. Soni, A. Tripathi, M. Shrotri, K. Agarwal, Opt. Quantum Electron. **55**(4), 384 (2023).
- [19] Y. K. Gupta, A. Goel, A. Tiwari, A. S. Das, Proceeding of International Conference on Innovations in High Speed Communication and Signal Processing, **IHCSP**, 398 (2023).
- [20] Y. K. Gupta, A. Goel, Wireless Personal Commun. **132**(4), 2563 (2023).
- [21] Y. K. Gupta, A. Goel, Heliyon **9**(2), e13325 (2023).
- [22] P. W. Kruse, L. D. Mcglauchlin, R. B. Mcquistan: Elements of infrared technology: Generation, transmission and detection, Wiley, (1962).
- [23] I. I. Kim, B. Mcarthur, E. J. Korevaar, Optical Wireless Communications III, Spie **4214**, 26 (2001).
- [24] J. Feng, X. Zhao, Optics Communications **402**, 340 (2017).
- [25] M. Singh, J. Malhotra, Opt. Quant. Electron. **51**, 1 (2019).
- [26] R. Ghalot, C. Madhu, G. Kaur, P. Singh, Wireless Personal Commun. **105**, 1215 (2019).

---

\*Corresponding author: yogesh.fetgkv@gmail.com